

CFTR Displays Voltage Dependence and Two Gating Modes during Stimulation

HORST FISCHER and TERRY E. MACHEN

From the Department of Molecular and Cell Biology, Division of Cell and Developmental Biology, University of California at Berkeley, Berkeley, California 94720

ABSTRACT The patch-clamp technique in conjunction with current noise analysis was employed to clarify the events underlying the regulation of the CFTR (cystic fibrosis transmembrane conductance regulator) during cAMP-dependent stimulation. 3T3 fibroblast cells expressing the CFTR were stimulated in cell-attached mode with forskolin. The number (N) of activated channels per patch ranged from 1 to ~ 100 . In true single-channel recordings, CFTR's gating was best described by two open states (~ 5 and ~ 100 ms) and three closed states (≤ 5 , ~ 100 , and $\sim 1,000$ ms). Current noise analysis resulted in spectra containing two distinct Lorentzian noise components with corner frequencies of 1.3 Hz and ~ 50 Hz, respectively. Single-channel time constants were dependent on voltage. The fastest closed state increased its contribution from 48% at +100 mV to 87% at -100 mV, and the medium open state reduced its length to one half, resulting in gating dominated by fast events. Similarly, the fast Lorentzian increased its amplitude, and its corner frequency increased from 44 Hz at +100 mV to 91 Hz at -100 mV, while the slow Lorentzian was voltage independent. In multi-channel recordings $N \cdot P_o$ (i.e., N times open probability) increased significantly, on average by 52% between -90 and $+90$ mV. Stimulation with forskolin increased P_o of CFTR to ~ 0.5 , which resulted from a decrease of the longest closed state while the faster open and closed states were unaffected. Neither corner frequency was affected during stimulation. Recordings from multichannel patches revealed in addition, unique, very long channel openings (high P_o mode, average 13 s). Channels exhibiting high P_o (i.e., $P_o \sim 1.0$) or low P_o (i.e., $P_o \sim 0.5$) gating modes were both present in multichannel recordings, and CFTRs switched modes during stimulation. In addition, the switch to the high P_o mode appeared to be a cooperative event for channel pairs. High forskolin concentration (i.e., $10 \mu\text{M}$) favored transition into the high P_o mode, suggesting a cellularly mediated regulation of modal switching due to a fundamental change in configuration of the CFTR. Thus, during stimulation the CFTR increased its activity through two distinct effects: the reduction of the long closed state and modal switching to the high P_o mode.

Address correspondence to H. Fischer, Department of Molecular and Cell Biology, Division of Cell and Developmental Biology, University of California at Berkeley, 235 Life Science Addition, Berkeley, CA 94720.

INTRODUCTION

Identification and sequencing of the gene encoding the cAMP-regulated epithelial Cl^- channel (Rommens, Iannuzzi, Kerem, Drumm, Melmer, Dean, Rozmahel, Cole, Kennedy, and Hidaka, 1989; Riordan, Rommens, Kerem, Alon, Rozmahel, Grzelczak, Zielenski, Lok, Plavsic, and Chou, 1989; Kerem, Rommens, Buchanan, Markiewicz, Cox, Chakravarti, Buchwald, and Tsui, 1989) paved the way for the investigation of its structure-function relationship. Owing to its role in the genetically inherited disease Cystic Fibrosis it has been named the cystic fibrosis transmembrane conductance regulator (CFTR). Expression of recombinant CFTR in various cell systems lacking the CFTR, e.g., monkey kidney cells (Dalemans, Barbry, Champigny, Jallat, Dott, Dreyer, Crystal, Pavirani, Lecocq, and Lazdunski, 1991), murine fibroblasts (Anderson, Rich, Gregory, Smith, and Welsh, 1991), Sf9 insect cells (Kartner, Hanrahan, Jensen, Naismith, Sun, Ackerley, Reyes, Tsui, Rommens, and Bear, 1991), frog oocytes (Bear, Duguay, Naismith, Kartner, Hanrahan, and Riordan, 1991), or its insertion into lipid bilayers (Tilly, Winter, Ostedgaard, O'Riordan, Smith, and Welsh, 1992) produced a small 6–10 pS ohmic Cl^- channel. Regulation of the kinetics of the CFTR has remained largely obscure due to a combination of its low conductance and its high abundance in the cell membrane. To overcome limitations of single-channel analysis, we (Fischer, Kreusel, Illek, Machen, Hegel, and Clauss, 1992) and others (Larsen, Gabriel, Fullton, Boucher, Price, and Stutts, 1992; Venglarik, Schultz, Frizzell, and Bridges, 1994) have applied current noise analysis to multi-channel or whole-cell patch clamp recordings for the analysis of regulation of CFTR. In addition, we recently described fluctuations due to cAMP-dependent Cl^- secretion across HT-29 epithelial monolayers (Fischer et al., 1992).

In this report, we present kinetic characteristics of the CFTR and its regulation during forskolin (i.e., cAMP-dependent) stimulation. All measurements were performed in the cell-attached mode (so as not to disrupt the channels' immediate environment) at 37°C (to measure its physiological gating). We have found that CFTR's gating is described by five states, of which three show voltage dependence, and one (the longest closed state) is regulated by forskolin thereby increasing P_o . In addition, forskolin induced a distinct high P_o gating mode of CFTR.

Parts of this report have been published previously in abstract form (Fischer and Machen, 1993).

MATERIALS AND METHODS

Cells

Mouse fibroblast NIH 3T3 cells stably transfected with the wild-type CFTR (Anderson et al., 1991) were grown in Dulbecco's minimal essential medium (H-21) supplemented with 10% newborn calf serum and 10^5 U/liter penicillin and 0.1 g/liter streptomycin (all from University of California at San Francisco Cell Culture Facility) in an atmosphere of 95% air/5% CO_2 at 37°C. Cells were passaged every 5–7 d in a 1:10 fashion. Cells were seeded on small glass cover slips (10-mm diam) and were used for experiments after 1–4 d.

Single-Channel Recordings

Cells were placed in an open, constantly perfused chamber (volume ~ 0.75 ml) on the stage of an inverted microscope (Nikon Diaphot). The distance between valve and chamber resulted in a dead time of ~ 30 s after solution change which was excluded from figures showing time courses of experiments. All measurements were performed at 37°C . Bath temperature was sensed and regulated by a DC-powered temperature controller (TC-1, N.B. Datyner Stony Brook, NY) with the help of both an inflow and a chamber heater (Datyner, Gintant, and Cohen, 1985).

Patch pipettes were pulled from thick-walled borosilicate glass (Corning 7052, World Precision Instruments, Sarasota, FL) and fire polished; when filled with NMDG-Cl solution, pipettes yielded resistances of 20–30 M Ω . All recordings in this report were performed in the cell-attached mode. Currents were amplified (Axopatch 1D, Axon Instruments, Foster City, CA), filtered at 500 Hz and sampled at 2 kHz (if not mentioned) continuously to a computer hard disk (PClamp, Axon Instruments). For display in some figures, the sampling frequency was numerically reduced as stated.

The analysis of true single-channel recordings was largely based on the description of Colquhoun and Sigworth (1983). Briefly, on the computer screen, two cursor lines were manually set to the displayed single-channel current levels. The 50% threshold between the cursors was used as a criterion for a channel event and for open- and closed-time estimations. Duration histograms were created by plotting the square root of the number of events versus logarithmically binned durations as described by Sigworth and Sine (1987). Histograms were fitted with the corresponding probability density function of the form

$$n = \sum_{j=1}^m a_j \cdot \exp [\ln t - \ln \tau_j - \exp (\ln t - \ln \tau_j)] \quad (1)$$

where τ and a are the respective time constants and the fraction of total events of the j th state. For closings, the number of fitted time constants ($m = 3$) defined a short, a medium, and a long closed time constant (τ_{cs} , τ_{cm} , τ_{cl}). For openings $m = 2$ defined short and medium open time constants (τ_{os} , τ_{om}).

All-point amplitude histograms were built from multichannel recordings containing few channels. Records sampled at 200 Hz and filtered at 50 Hz were used. Histograms were fitted with multiple Gaussian distributions whose relative weights were used to estimate the probability of each current level, P_r . For independent gating channels P_r follows a binomial distribution of the form

$$P_r = \frac{N!}{r! \cdot (N-r)!} P_o^r \cdot (1 - P_o)^{N-r} \quad (2)$$

where $r = 0, 1, \dots, N$. Fits yielded the channels individual open probability, P_o , and the number of channels, N . Fits were performed as 1-parameter fits with a fixed N and repeated for different N -values to reveal the best fit.

Variance Analysis

The majority of recordings were from patches containing multiple channels. Multichannel recordings were variance analyzed. From recorded current noise spectra the bandwidth of channel gating was estimated (< 200 Hz for positive, and < 400 Hz for negative potentials), and traces were digitally low-pass filtered to remove nonspecific high-frequency noise. The mean current (I) and its variance (σ^2) were calculated from consecutive 10-s intervals. Number of channels (N) and P_o were calculated from variance data with (Ehrenstein, Lecar, and Nossal,

1970)

$$\sigma^2 = I \cdot i \cdot (1 - P_o) \quad (3)$$

and

$$I = N \cdot i \cdot P_o \quad (4)$$

Eq. 3 and 4 report N and P_o independent of the number of kinetic states of channel gating. Because all other variables are known in a patch clamp measurement, N and P_o are determined. The digital filter was designed following the source code published by Colquhoun and Sigworth (1983), and the response of two filters in series was taken into account. Programs for calculation of I and σ^2 , and the reduction of sampling frequencies for plotting overview recordings were developed by one of the authors (H. Fischer). Cl^- moving into the cell is reported as positive current and refers to upward deflections in the figures. Voltages (V) are given as negative pipette potentials referring to the bath with respect to the pipette. The liquid junction potential resulting from nonsymmetrical solutions in bath and pipette was insignificant (0.15 ± 0.28 mV, $n = 28$).

Stationary Noise Analysis

One current output of the patch amplifier was modified with a simple RC high-pass element ($R = 210$ k Ω , $C = 22$ μF , resulting in a -3 -db attenuation at 0.034 Hz) to yield the AC component of the current only. Then the signal was low-pass filtered at 400 Hz (Frequency Devices, Inc., Haverville, MA), and periods of 4096 points were sampled at 1 kHz by a separate computer using software developed for acquisition and analysis of current fluctuations (W. Van Driessche, University of Leuven, Belgium). The time-domain signal was on line fast Fourier transformed, resulting in a spectrum of current fluctuations. Spectra were calculated in a bandwidth of 0.25–400 Hz and were numerically corrected for the characteristics of the high-pass element with a frequency-dependent correction factor $c = 1 + 1/(\text{RC} \cdot 2\pi f)^2$. With increasing frequencies c quickly approaches 1. Spectra from 10 consecutive recording periods were averaged and stored on hard disk.

Spectra were fitted off-line with the sum of two Lorentzian noise components (Lindemann, 1980; Van Driessche and Zeiske, 1980)

$$S(f) = S_{0l}/[1 + (f/f_{cl})^2] + S_{0h}/[1 + (f/f_{ch})^2] \quad (5)$$

to estimate the Lorentzian parameters, the plateau (S_0) and the corner frequency (f_c). The indices l and h denote the low- and high-frequency Lorentzian, respectively. $S(f)$ is the spectral density at the frequency f . In some cases, high-frequency points were omitted due to increasing nonspecific noise. No data points were disregarded at the low-frequency end of the spectra. Line frequency (60 Hz) and multiples of it were excluded from fits. The fit algorithm was described previously (Van Driessche and Zeiske, 1980) and is a compromise between the Newton-Raphson, steepest descent, and Marquard algorithm. Data in this report are presented as original values or as means \pm SEM, and were described and compared by standard statistical testing (t tests, regression analyses).

Solutions

The composition of the bath solution was (in millimolar): 141 NaCl, 4 KCl, 1 KH_2PO_4 , 1 MgCl_2 , 1.7 CaCl_2 , 10 HEPES, 25 glucose, pH = 7.4. Pipette filling solution was (in millimolar): 147 N -methyl-D-glucamine chloride (NMDG-Cl), 1.7 CaCl_2 , 10 HEPES, 25 glucose, pH = 7.4. Forskolin (Calbiochem-Novabiochem Corp., La Jolla, CA), an adenylyl cyclase activator, was made as a 10-mM stock in dimethyl sulfoxide and used at 10 pM to 10 μM .

RESULTS

The expression of CFTR in permanently transfected NIH 3T3 cells was quite variable from cell to cell and ranged from 1 to ~ 100 channels per patch after stimulation. This variability was independent of the pipette resistance and, therefore, likely the membrane area, and was also independent of the cells' passage number or days in culture. The majority of recordings were from multichannel patches. Only 4 out of 55 patches were true single-channel recordings which showed the consistent presence of one open level after maximal stimulation with $10 \mu\text{M}$ forskolin. Only those recordings were used for the estimation of time constants on the single-channel level. All CFTR recordings in this report are from cell-attached patches, because excision significantly altered channel gating (see Discussion). All cells were stimulated with forskolin after seal formation. Dibutyryl-cAMP (2 mM) similarly stimulated the cell-attached CFTR, but it was less effective and needed longer incubation times (2–3

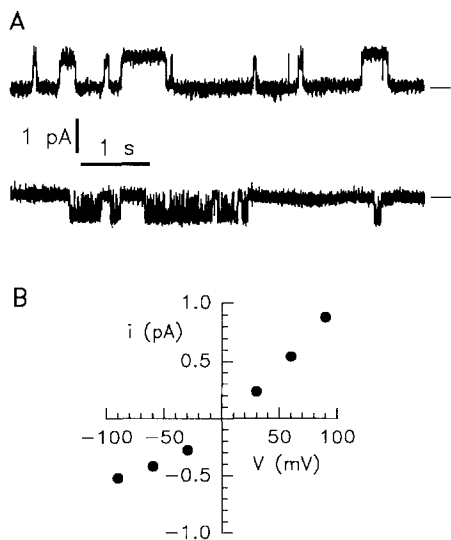


FIGURE 1. Current-voltage characteristics of the cell-attached CFTR. (A) Current traces were recorded from a cell previously stimulated with $10 \mu\text{M}$ forskolin at $+100 \text{ mV}$ (*upper trace*) and -100 mV (*lower trace*). Potentials refer to the bath with respect to the pipette. Pipette contains NMDG-Cl solution. Closed state is marked with a dash. Filtered at 200 Hz . (B) Single-channel current-voltage relation. Rectification of single-channel currents (i) is due to nonsymmetrical Cl^- concentrations in cell-attached mode. Slope conductance at 0 mV was $g_0 = 8.5 \text{ pS}$.

min) before channels were activated (not shown). Stimulation of silent, cell-attached patches allowed us to verify the zero-current baseline and directly probe the cAMP-sensitivity of the recorded channels, since we had to take into account that CFTR-like, non-cAMP-dependent Cl^- channels have also been found in the NIH 3T3 parent cell line (Gabriel, Price, Boucher, and Stutts, 1992).

Voltage-dependent Gating of CFTR

Current traces recorded from a single, forskolin-stimulated CFTR at $+100 \text{ mV}$ and at -100 mV are shown in Fig. 1. CFTR's gating was clearly voltage-dependent. At positive potentials (Fig. 1 A, *upper trace*) long openings and closings dominated while at negative potentials (*lower trace*) additional fast closures were present. Visual inspection of the current traces shows that both slow and fast gating was present at

both potentials, though they were expressed differently at positive vs negative potentials.

CFTR's current-voltage (I/V) relation (Fig. 1 *B*) showed rectification of the single-channel current due to an appreciable Cl^- concentration gradient across the channel ($\sim \text{Cl}_{\text{in}}^-:\text{Cl}_{\text{out}}^- = 50:150$) in cell-attached mode. Therefore, currents were voltage dependent in our recordings. In excised patches, the channel was linear in symmetrical solutions with a single-channel conductance of $g = 10.4 \pm 0.5$ pS ($n = 7$). The reversal potential in cell-attached mode was, on average, indistinguishable from zero, and, thus, applied potentials were considered as the net driving force for Cl^- .

Visual examination of current traces (Fig. 1 *A*) of CFTR's gating indicated distinct slow and fast events for the open and the closed times. The statistical distributions of open and closed times are shown in Fig. 2. Histograms of the closed times (Fig. 2 *A*)

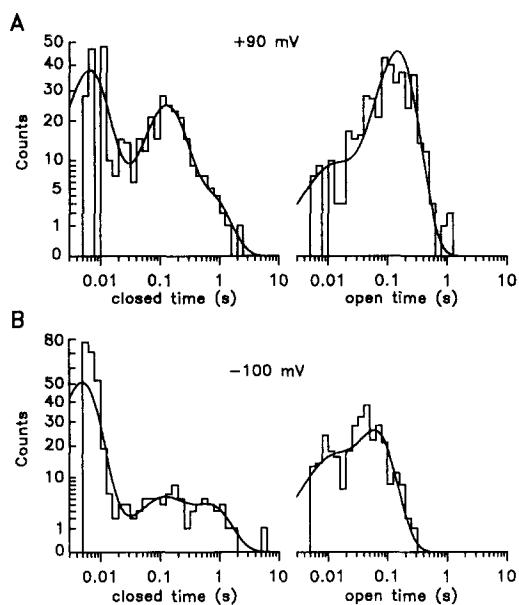


FIGURE 2. Single-channel kinetics of the CFTR in cell-attached mode. (*A*) Dwell time histograms at positive potential ($V = +90$ mV). Closed time distributions were best described by three exponentials. Fitted time constants (and number of events) were: $\tau_{\text{cs}} = 6.0$ ms (224), $\tau_{\text{cm}} = 112$ ms (124), $\tau_{\text{cl}} = 616$ ms (30.8). Open time distribution was fitted with two exponentials: $\tau_{\text{os}} = 7.5$ ms (27.6), $\tau_{\text{om}} = 147$ ms (339). (*B*) Dwell time histograms at negative potential ($V = -100$ mV). Fitted time constants of the closed time distribution were: $\tau_{\text{cs}} = 4.8$ ms (350), $\tau_{\text{cm}} = 85.6$ ms (18.3), $\tau_{\text{cl}} = 641$ ms (30.0). Fit of open time distribution resulted in: $\tau_{\text{os}} = 6.0$ ms (36), $\tau_{\text{om}} = 59.4$ ms (192). τ_{om} was significantly shorter and τ_{cs} showed significantly increased counts (at the

expense of τ_{cm}) at negative potentials (see Table I). Note that τ_{cs} lies at the edge of the employed bandwidth and is likely shorter. Stimulated with $1 \mu\text{M}$ forskolin; current record was filtered at 200 Hz.

showed a triple exponential, and of the open times (Fig. 2 *B*) a double exponential distribution, indicating two distinct open and three closed states for the CFTR. All exponents lay well apart and were readily distinguished allowing reliable fits of the time constants. Table I quantifies CFTR's gating characteristics. At positive potentials (+90 mV and +100 mV data were pooled; see Table I, Fig. 2 *A*) the lifetimes of the three closed states were, on average, 5, 150, and 1,700 ms; the two open states showed average lifetimes of 5 and 118 ms. Note that the 5-ms closed time constant is likely even shorter because this lay at the limit of our single-channel event analysis (filtered at 200 Hz) and was fitted poorly. Nonspecific noise did not allow us to use the full bandwidth of recordings (500 Hz).

The applied voltage significantly affected time constants and their amplitudes such that fast gating was favored at negative potentials (-100 mV). Comparing Fig. 2, *A* and *B*, displays this effect. At -100 mV, the short closed state emerged as the dominating closing state increasing its contribution from, on average, 48% (at $+90/+100$ mV) to 87% of all closings (Table I). This happened at the expense of the medium closing state (Fig. 2 *A*), which significantly reduced its amplitude from, on average, 34 to 6% at -100 mV (Table I). None of the closed time constants changed its mean lifetime in dependence of the applied voltage.

At the same time, the medium open time significantly decreased its mean lifetime from, on average, 118 ms (at $+90/+100$ mV) to 63 ms at -100 mV. The apparent reduced amplitude of the medium open state at -100 mV (Fig. 2 *B*) was not significantly different from that exhibited at positive potentials (Table I). The time constant of the fast open state showed no voltage-dependence (Table I). Despite a

TABLE I
Single-Channel Kinetics

| <i>V</i> | Openings | | Closings | | |
|-----------|-------------------------|-----------------|-----------------|----------------|----------------|
| | Short | Medium | Short | Medium | Long |
| <i>mV</i> | | | | | |
| +90/100 | τ 5.5 \pm 0.6 | 118 \pm 9.8 | 5.6 \pm 0.4 | 150 \pm 29.9 | 1687 \pm 464 |
| | <i>a</i> 27.8 \pm 3.5 | 66.6 \pm 5.2 | 47.5 \pm 2.0 | 33.7 \pm 1.6 | 18.3 \pm 2.7 |
| -100 | τ 6.2 \pm 0.9 | 62.7 \pm 3.3* | 4.9 \pm 0.15 | 119 \pm 9.1 | 675 \pm 34.5 |
| | <i>a</i> 17.4 \pm 1.7 | 82.7 \pm 1.7 | 87.1 \pm 0.9* | 5.7 \pm 1.1* | 7.3 \pm 0.2 |

Time constants (τ in milliseconds) and fraction of total events (*a* in percent) were estimated by fitting Eq. 1 to open and closed time distributions. Data are from four different cells with $n = 4$ records at $+90$ mV, $n = 3$ at $+100$ mV ($+90$ and $+100$ mV data were pooled), and $n = 2$ at -100 mV (recordings at -100 mV are from the same patches which were studied at $+100$ mV); stimulated with 1–10 μ M forskolin. Average number of events in analyzed recordings was 562 ± 86 . Time constants from these nine recordings entered into Fig. 7. Event lengths were measured on records filtered at 200 Hz. *Significantly different with $p < 0.05$. $P_0 = 0.33 \pm 0.08$ at $+90/+100$ mV and 0.32 ± 0.06 at -100 mV for recordings in this table.

strong voltage dependence of gating kinetics, P_o of single channels showed no difference (0.33 ± 0.08 at $+90/+100$ mV [seven records] and 0.32 ± 0.06 at -100 mV [two records]) which may, however, be obscured by the wide P_o -range in these recordings (0.03 to 0.53, see also Fig. 7).

Current noise spectra also provided evidence for the voltage-dependent gating of the CFTR. Unlike the kinetic analysis of open and closed times of single-channel records, analysis of current fluctuations allows the determination of channel kinetics from both single- and multichannel recordings. Most of our patches contained multiple CFTRs, reaching a maximal conductance after stimulation of up to $G = 1$ nS.

Fig. 3 *A* shows a multichannel recording after forskolin stimulation at $+100$ mV and -100 mV. Slow "wavelike" gating (Bear et al., 1991) dominated at positive potentials, while fast gating was more prevalent at negative potentials as shown for

the single CFTR (Fig. 1). In the frequency domain, this gating behavior translated into the low- and high-frequency Lorentzians, which lay well apart, allowing accurate determination of their corner frequencies. Spectra from both single-channel recordings and multichannel recordings resulted in comparable corner frequencies. The

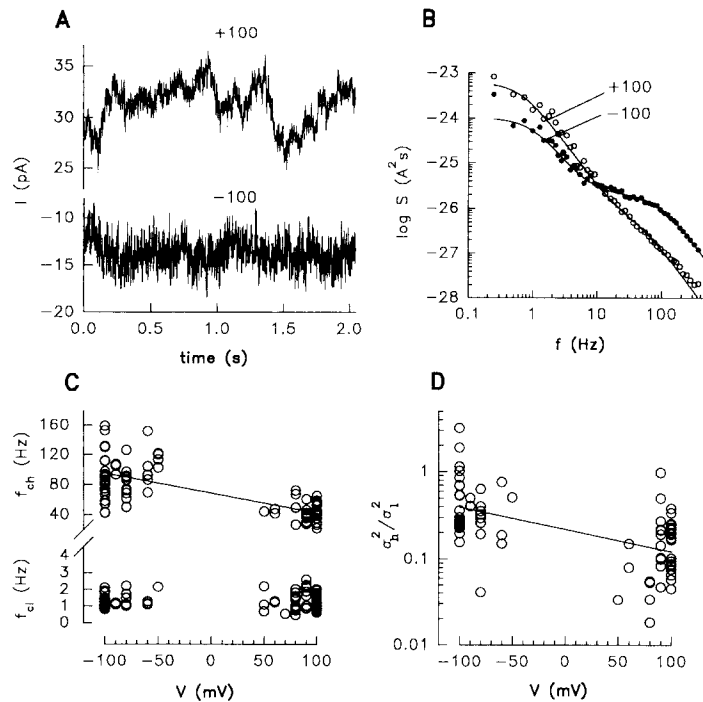


FIGURE 3. Voltage-dependence of kinetics in multichannel recordings. (A) Two current sweeps from a stimulated ($10 \mu\text{M}$ forskolin), cell-attached patch. At $+100 \text{ mV}$ (upper trace) the presence of a low frequency component is obvious. At -100 mV (lower trace, recorded 60 s later from the same patch), fast-frequencies dominated the gating. Filtered at 500 Hz. (B) Current noise spectra of recordings in A. Lorentzian parameters were (f_{cl} , f_{ch} , S_{0l} , S_{0h}): 0.69 Hz, 45.9 Hz, $6.01\text{E-}24 \text{ A}^2\text{s}$, $5.24\text{E-}27 \text{ A}^2\text{s}$ at $+100 \text{ mV}$; and 1.02 Hz, 91.1 Hz, $987\text{E-}27 \text{ A}^2\text{s}$, $20.7\text{E-}27 \text{ A}^2\text{s}$ at -100 mV . (C) Voltage dependence of Lorentzian corner frequencies. The low-frequency Lorentzian's f_c was independent of V and averaged 1.33 ± 0.05 , $n = 88$. The fast Lorentzian's f_c was significantly dependent on V (unpaired data, Spearman's rank correlation: $Z = -6.11$, $n = 83$, $p < 0.001$). n refers to the number of fitted spectra each of which is an average of 10 consecutive spectra (see Methods). (D) The ratio of the high-frequency to the low-frequency Lorentzian (σ_h^2/σ_l^2) was dependent on the potential, indicating significantly increased high-frequency noise at negative V ($Z = -4.37$, $n = 72$, $p < 0.001$). Average ratio at -100 mV was $64.5 \pm 15.6\%$ ($n = 21$) and at $+100 \text{ mV}$ $17 \pm 2.2\%$ ($n = 19$). σ^2 was calculated for each Lorentzian as $\sigma^2 = S_0 f_c \cdot \pi/2$.

slow corner frequency did not vary with voltage and averaged $f_{cl} = 1.33 \pm 0.05 \text{ Hz}$ ($n = 88$). At negative potentials the amplitude of the high-frequency Lorentzian was significantly increased despite an attenuation of the slow Lorentzian due to reduced single-channel amplitudes in the cell-attached mode (Fig. 3 B). Thus, the high

frequency Lorentzian was much more prominent than the low frequency Lorentzian under these conditions. At the same time, the fast Lorentzian increased its frequency from $f_{\text{ch}} = 43.7 \pm 7.73$ Hz ($n = 19$) at +100 mV to $f_{\text{ch}} = 90.8 \pm 6.76$ Hz ($n = 22$) at -100 mV. Fig. 3 C summarizes the data for all fitted corner frequencies, showing the voltage-dependence of f_{ch} ($p < 0.001$) and the unchanged f_{cl} . Fig. 3 D quantifies the voltage-dependence of the fast Lorentzian relative to the slow Lorentzian, and shows that there was considerably more high frequency noise at negative as compared to positive potentials.

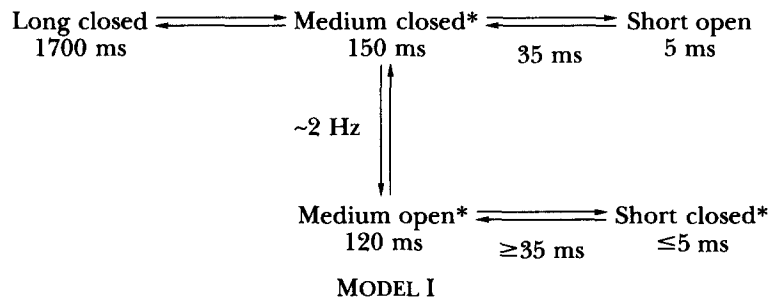
In several previous reports of CFTR currents in whole cell or excised single-channel recordings, currents were shown to be voltage-independent (e.g., Cliff and Frizzell, 1990, Haws, Krouse, Xia, Gruenert, and Wine, 1992). With the strong voltage dependence of gating kinetics in our cell-attached recordings, an effect on the P_o seemed likely. Fig. 4 shows two typical current traces (*top*) recorded at -60 and +60 mV from a stimulated cell. Visual examination of traces and amplitude histograms (*middle*) reveal four visible current levels (i.e., one closed and three open levels) at -60 mV and five current levels at +60 mV (i.e., one closed and four open levels). The probability for each level was estimated from Gaussian fits to the amplitude histograms. Current level probabilities (*bottom*) were fitted well to a binomial distribution resulting in estimates for P_o of the individual channel and their number (N) in the current traces: $P_o = 0.170 \pm 0.0011$ and $N = 3$ at -60 mV, and $P_o = 0.215 \pm 0.0072$ ($p < 0.001$) and $N = 4$ at +60 mV (Fig. 4). Therefore, both P_o and N , as determined from amplitude histograms, were significantly increased at positive potentials.

With larger N the determination of P_o and N from amplitude histograms becomes increasingly unreliable (Sachs, Neil, and Barkakati, 1983). Therefore, we calculated $N \cdot P_o$ from the total current/single-channel current ratio (I/i , Eq. 4) from I/V ramps. Fig. 5 shows a typical I/V ramp recorded from a stimulated cell. Voltage-steps were applied as indicated in Fig. 5 A. The dependence of I , i , and the seal current on the potential are shown in Fig. 5 B. These data were used to calculate $N \cdot P_o$ for each voltage (Fig. 5 C). $N \cdot P_o$ was significantly related to V with $N \cdot P_o = 5.7 + 0.0092$ [mV^{-1}] $\cdot V$ [mV], $r = 0.887$, $p < 0.05$ for this recording. The slope of this voltage-dependent relation averaged for 18 experiments with comparable currents 0.00611 ± 0.0025 mV^{-1} (significantly different from zero, $p < 0.05$) ranging from -0.009 mV^{-1} to 0.025 mV^{-1} , and $N \cdot P_o$ at 0 mV was 2.66 ± 0.48 ($n = 18$). Therefore, $N \cdot P_o$ increased on average by 52% between -90 and +90 mV. As shown in Fig. 4 this voltage dependence is due to changes in both N and P_o .

A Gating Model for the CFTR

Single-channel analysis of CFTR's gating gave evidence for three closed and two open states (Fig. 2, Table I), which theoretically could give rise to multiple Lorentzians in the spectra. Within the analyzed frequency-range (0.25–400 Hz) we resolved two distinct Lorentzians. Modeling of CFTR's gating allows several different linear or branched schemes which would predict different Lorentzians. We favor the

following model as a good approximation of both single-channel and spectral data:



Approximate mean lifetimes of states are given in ms for positive potentials. Lorentzian corner frequencies (in Hz) for this model can roughly be predicted with $2\pi f_c = 1/\tau_o + 1/\tau_c$, voltage-dependent states are starred. This model predicts one Lorentzian at ~ 2 Hz and two at ≥ 35 Hz for positive potentials. The predicted slow Lorentzian is likely somewhat slowed due to the influence of the long closed state, which is not likely to generate a separate, distinct Lorentzian due to its long time constant and its low incidence (Fig. 2A). At positive potentials, the two fast Lorentzians predicted from single-channel gating are likely to merge to the one observed high-frequency Lorentzian. The voltage-dependence of the medium open and the short closed states (Table I) predict for negative potentials an increase in f_c (due to the shorter medium open state) and an increase in S_0 (due to the increased incidence of the short closed state), and therefore, likely account for the effects of voltage on both the increased f_c and S_0 of the observed high-frequency Lorentzian (Fig. 3D). At negative potentials the incidence of the medium closed state is greatly reduced (Fig. 2B and Table I) and, thus, is not likely to be a significant part of the fast Lorentzian any more. This five-state gating model obtained from the single-channel kinetics is therefore consistent with the observed double-Lorentzian in the current noise spectra.

The sequence of this model is also consistent with observations obtained from close inspection of the current traces (e.g., Fig. 1): (a) short openings are reached from the medium closed state, and, (b) similarly, medium openings are broken by short closures; (c) the medium open and the medium closed state appear to be directly connected. The long closed state, which may represent the inactive channel, is probably connected to the medium closed state. Although this model describes our observations reasonably, other gating models are possible. For example, the short open and the short closed state may be connected directly, which would result in a voltage-dependent Lorentzian with $f_c \geq 63$ Hz.

Effects of Forskolin Stimulation: Reduction of the Long Closed State

Addition of forskolin to cell-attached patches reliably activated silent patches. Concentrations as low as 10 pM activated the CFTR while 1 μ M was needed for maximal effects. We applied 1 or 10 μ M to elicit maximal responses. Fig. 6 shows a stimulation of a patch containing a single CFTR. No channel activity was present for

~80 s before stimulation. After addition of forskolin and an initial brief latent period of, on average, 30–40 s, one channel activated and gated continuously (here shown for 8 min). Fig. 6 B shows a detail from the overview trace in Fig. 6 A displaying similar kinetics as shown before (e.g., Fig. 1). During this stimulation the P_o quickly

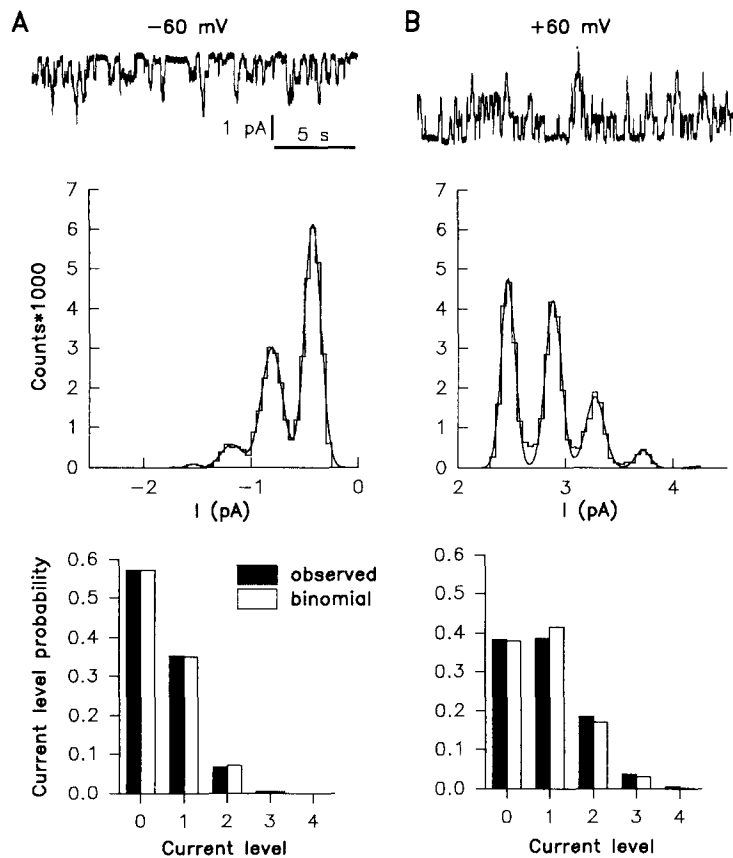


FIGURE 4. Amplitude histograms at -60 and $+60$ mV as indicated. Traces were filtered at 50 Hz, sampled at 200 Hz, length is 20 s, stimulated with $1 \mu\text{M}$ forskolin. Trace in *A* was recorded 10 s after trace *B* from the same patch. (*A*) Current trace and corresponding amplitude histogram (*middle*) and current level probability plot (*bottom*) at -60 mV. Histogram was fitted with 4 Gaussian distributions yielding the relative probabilities for each current level. Binomial fit (*open bars, bottom*) of current level probabilities (*filled bars*) resulted in $P_o = 0.170 \pm 0.0011$ and $N = 3$. (*B*) Current trace, amplitude histogram, and current level probability plot at $+60$ mV. Amplitude histogram was fitted with 5 Gaussians. Binomial fit of current level probabilities resulted in $P_o = 0.215 \pm 0.0072$ and $N = 4$.

increased and averaged 0.50 ± 0.02 after stimulation; maximal P_o (within 4.1-s intervals) in this record was 0.83.

To analyze the contribution of each gating state to the regulated P_o after stimulation, the mean time spent in each state ($a\tau$) was plotted vs P_o . For nine single

channel records, the P_o was calculated and $a \cdot \tau$ was estimated from fits of respective closed and open time histograms. Interestingly, only the long closed state (τ_{cl}) showed a significant relation to P_o (Fig. 7 A, filled circles). All other open and closed states (Fig. 7, A and B) were not related significantly to P_o indicating that CFTR was stimulated by reducing the frequency and length of the longest closed state. Note that the medium open state (squares) and the medium closed state (open circles) showed some relationship to P_o , but this could not be statistically established.

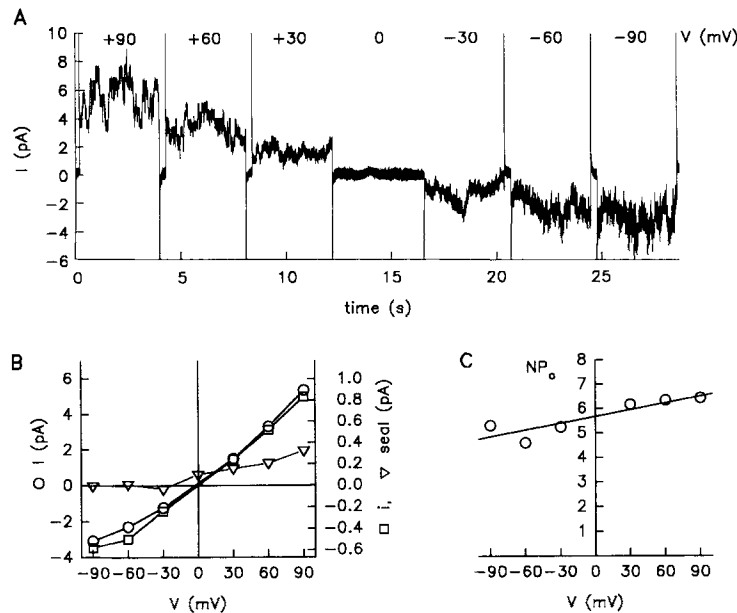


FIGURE 5. Current-voltage relation and $N \cdot P_o$ vs voltage plot. (A) Stepwise current ramp from +90 to -90 mV as indicated. Voltage steps were clamped for 3.8 s and were separated by 0.3 s intervals at 0 mV. Filtered at 150 Hz. Note the voltage-dependent current fluctuations. From the current trace I was calculated as the average current during the voltage-pulse (omitting the initial capacitive transient) minus the seal current. The seal current was measured from the closed level, if possible, or from I/V relations before stimulation. (B) Mean current I (circles), single-channel current i (squares), and seal current (triangles) as a function of applied voltage from trace in A. (C) $N \cdot P_o$ vs V plot. $N \cdot P_o$ was calculated from I/i from values in B. Regression line is significant with $N \cdot P_o = 5.7 + 0.0092 [mV^{-1}] \cdot V [mV]$, $r = 0.887$, $p < 0.05$.

The long closed state may be the inactive state of the channel, although we cannot exclude an additional inactive state different from the long closed state we have observed and quantified as part of the gating process of CFTR. The simplest interpretation of our data is that forskolin stimulation of the cells activates the CFTR (likely through a phosphorylation event) through a single process, i.e., the reduction of the long closed state, resulting in values for $P_o \sim 0.5$.

Effects of Forskolin Stimulation: Cooperative, Very Long Openings

In recordings in which single-channel events could be discerned, stimulation often not only increased P_o and N , but also provoked very long open times of the channels.

Two examples of forskolin stimulation of patches with two and four active channels are shown in Fig. 8. Both traces (Fig. 8, *A* and *B*) started out silent. During stimulation, periods of very long openings were observed, averaging 13.2 ± 3.4 s ($n = 11$) and ranging from 3.4 to 34.6 s. In all cases, the very long openings occurred as a coordinated opening of two channels, as shown in Fig. 8. During the very long open times, there were few brief closures. Replotting the same data at higher time resolution (Fig. 8 *C*) displays this clearly. Since we never observed very long open

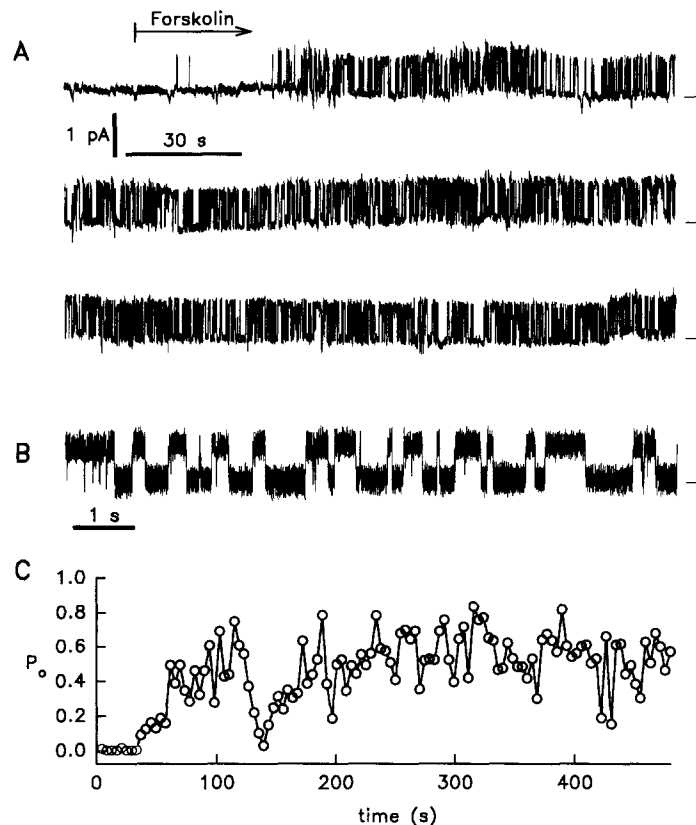


FIGURE 6. Stimulation of a cell-attached recording of a single CFTR. (*A*) 8-min continuous current recording during stimulation with forskolin ($1 \mu\text{M}$). Sampled at 50 Hz; $V = 90$ mV; (*dashes*) closed state. (*B*) Detail from the overview trace in *A*. Filtered at 200 Hz. (*C*) P_o of current trace shown in *A*. P_o was calculated as I/i from 4.096 s intervals. Average $P_o = 0.50 \pm 0.02$; maximal $P_o = 0.83$.

times in true single-channel records (for a total time of 22 min of recordings of single CFTRs; eg, Fig. 6), it appeared that the channels could reach a stable long open state only in multichannel patches. Note that during very long openings, the channels changed their gating behavior suddenly from a low P_o mode with independently gating channels to a cooperative high P_o locked-open mode which was either

sustained (Fig. 8A) or reversed back to the low P_o mode (Fig. 8B). Both gating modes could coexist in the same patch (Fig. 8A), or the high P_o mode was entered only temporarily (Fig. 8B) indicating transitions between distinct gating modes.

The distribution of current amplitudes of multichannel recordings is expected to follow a binomial distribution (Eq. 2) if (a) all channels show the same gating, and (b) channels gate independently (Ehrenstein et al., 1970). Fig. 4 showed amplitude histograms of a stimulated patch in which these predictions were satisfied. The distribution of the probabilities of each current level (Fig. 4, filled bars, bottom) fit well to a binomial distribution (open bars) indicating independent gating in this recording. The fitted P_o -values (0.170 and 0.215, respectively) are indicative for the low P_o gating mode.

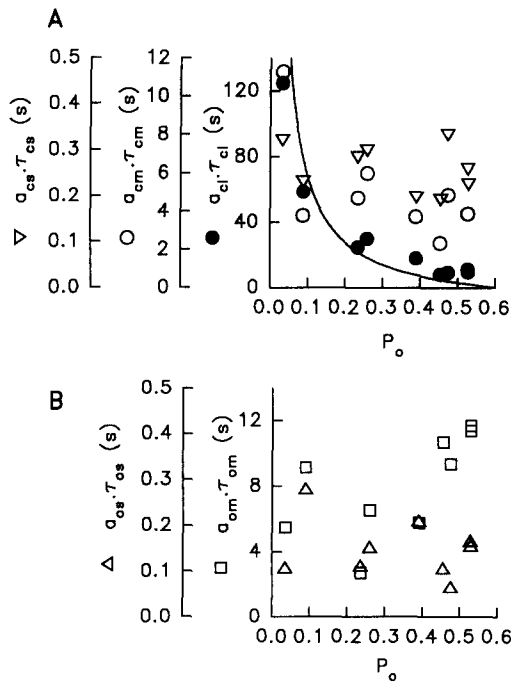


FIGURE 7. Relation of the times spent in different states of the cell-attached CFTR at different P_o . (A) Closed states. (B) Open states. Data points were calculated from a (in percent of total events) $\cdot \tau$ (in s) from parameters of fitted time histograms, and P_o was calculated from single-channel analysis. $a \cdot \tau$ is a measure of the relative mean time spent in a particular state. The long closed state (filled circles) showed a significant relation with P_o while all other open and closed states were unrelated. The continuous line shows for comparison a model described by $P_o = A / (B + (a_{cl} \cdot \tau_{cl}))$, where $A = (a_{om} \cdot \tau_{om}) + (a_{os} \cdot \tau_{os})$ and $B = A + (a_{cm} \cdot \tau_{cm}) + (a_{cs} \cdot \tau_{cs})$, and all other states are constant (and equal to the respective means of the observed states).

In contrast, the amplitude histogram in Fig. 9B (constructed from the current trace in Fig. 8A) deviated strikingly from a binomial (Fig. 9B, right), as predicted if the two different gating modes coexisted in this record. Thus, CFTR gated independently in the low P_o mode but not after modal switching.

P_o , N , and the Gating Mode Are Regulated during Stimulation

Cl^- secretion from a cell might be regulated through continuous changes in P_o and/or number of channels (N). Having shown that the CFTR exists in two gating modes introduces another possibility for the regulation of Cl^- secretion: the CFTR might be regulated by switching from the low P_o mode to the high P_o mode. The contribution of these different regulatory mechanisms was investigated using variance

and noise analysis on multichannel recordings, where a high degree of cooperativity (and, thus, transitions between modes) might be expected.

An example using a maximal concentration (10 μM) of forskolin for stimulation of a cell-attached patch containing many CFTRs is shown in Fig. 10. The overview trace in Fig. 10 *A* shows the profound stimulation of current across the membrane patch, and Fig. 10 *B* shows details taken from the overview trace at 41 s (Fig. 10 *B*, *top*) and at 276 s (Fig. 10 *B*, *bottom*). During unstimulated conditions, the channels showed independent gating with an obviously low P_o . Stimulation induced a sudden current peak, and then the current stabilized at an intermediate level with ~ 22 active channels (see further, Fig. 11 *D*). Current fluctuations increased at the same time (Fig. 10 *B*, *bottom*).

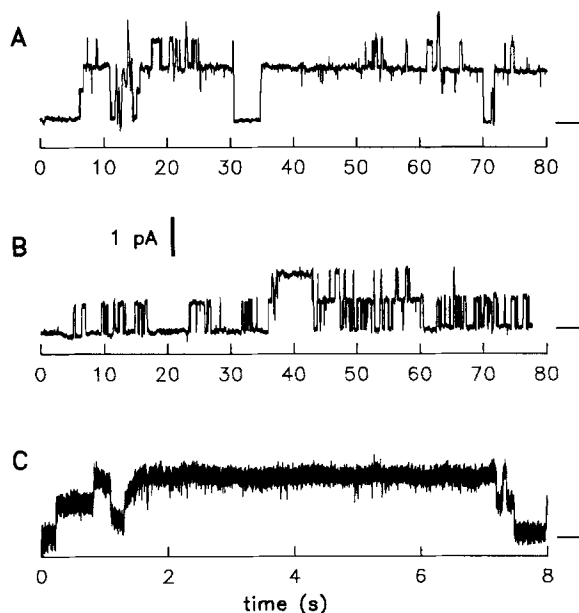


FIGURE 8. Stimulation of cell-attached, multichannel patches with forskolin (10 μM) results in cooperative, very long open times. (*A*) Four-channel patch showing continuously open channels (high P_o) and gating channels (low P_o) at the same time. (*B*) Stimulation activates at first one single channel. Activation of the second channel triggers a cooperative, very long opening of both channels. *A* and *B* are recordings from two different cells at $V = 80$ mV; sampled at 100 Hz; closed state is marked with a dash; X-axes are at $I = 0$. (*C*) Long opening of *B* (at 40 s) plotted at 300 Hz bandwidth. Opening is interrupted by only a few brief closures. Very long openings were also observed at negative potentials (not shown).

Current noise spectra recorded at the times indicated by the symbols in the overview trace are displayed in Fig. 11 *A* (symbols are corresponding). Under control conditions (*circles*), after stimulation (*triangles*), and after a time-dependent inactivation of current (*squares*), each spectrum exhibited two Lorentzians. The Lorentzian amplitudes increased with stimulation whereas the corner frequencies were independent of current and extent of stimulation. These findings are consistent with the single-channel data, where all states in the frequency range of noise analysis were unaffected by stimulation. It should be noted, however, that the long closed state as well as the very long openings did not contribute to the spectra. Therefore, the regulation of current in this multichannel record may have occurred through

regulation of the long closed state and by modal switching (i.e., from low P_o to high P_o).

To clarify how N and P_o were regulated during stimulation, we applied variance analysis (Sigworth, 1980). Since the two gating modes were expected to coexist in multichannel recordings, we used the current variance as a tool to distinguish between channels in the low P_o mode (which due to its gating generated the current variance), and the high P_o mode (which, due to its absence of gating, contributed little to the variance).

The variance data (σ^2) calculated from consecutive 10-s intervals of the entire current trace in Fig. 10 *A* are plotted in Fig. 11 *B* versus the mean current (I). σ^2 -values of this recording were in general very low and increased only slightly during the large stimulation of current, indicating that a considerable part of the current was carried by channels that did not contribute to σ^2 , e.g., channels in the high P_o mode.

The relation of the average P_o and N to I during stimulation with 10 μM forskolin is shown in Fig. 11, *C* and *D*. P_o and N were calculated from σ^2 data (Fig. 9 *B*) with Eqs. 3 and 4. As current increased channels switched into the high P_o mode,

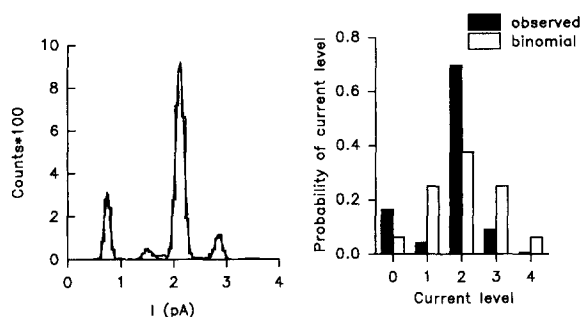


FIGURE 9. Amplitude histogram of current trace in Fig. 8 *A* (left) and current level probability plot (right). The second open level is over-expressed while the first, third, and fourth open level have a very low incidence (filled bars) deviating drastically from the binomial distribution (open bars) which is shown for comparison for $P_o = 0.5$ and $N = 4$. $V = 80$ mV, 10 μM forskolin.

increasing the average P_o to very high values. In this circumstance there was a close correlation between N and I , indicating that N was now the major regulator of current (Fig. 11 *D*). Although the calculated N and P_o represent averages and do not distinguish between the two gating modes, using reasonable assumptions, the contribution of the channels in the two gating modes to the total stimulated current can be estimated. For example, assuming an average $P_o = 0.5$ for the low P_o mode, the current carried by the low P_o channels is (Eq. 3) $I = \sigma^2/[i \cdot (1 - P_o)] = 3.1$ pA, and using (Eq. 4) $N = I/(i \cdot P_o) = 7.3$ channels (data from Fig. 10 *B*, legend). The rest of the current ($I = 13$ pA) is carried by 15.3 channels in the high P_o mode ($P_o \sim 1.0$). Thus, after stimulation roughly 2/3 of the channels in this recording (Fig. 10) were in the high P_o gating mode and 1/3 were in the low P_o mode.

Thus, for the recording shown in Fig. 10, forskolin increased current by initially regulating the P_o of low P_o channels. After CFTRs switched to the high P_o mode, current was regulated primarily through changes of N indicating that channels were recruited from an electrically silent pool. This may include (a) channels with an extremely low P_o that they did not contribute significantly to the current, (b) channels

present in the membrane but inactive, or (c) channels not present in the membrane, activated from a submembrane vesicle pool. Our measurements can not distinguish between these possibilities.

Modal switching appeared to be dependent on the agonist concentration. A low-dose forskolin stimulation (10 nM) is shown in Fig. 12. The overview trace (Fig. 12 A) shows the activation and inactivation of current across the cell-attached patch. Initially (Fig. 12 B, *top*), channels appeared to gate independently. Note, however,

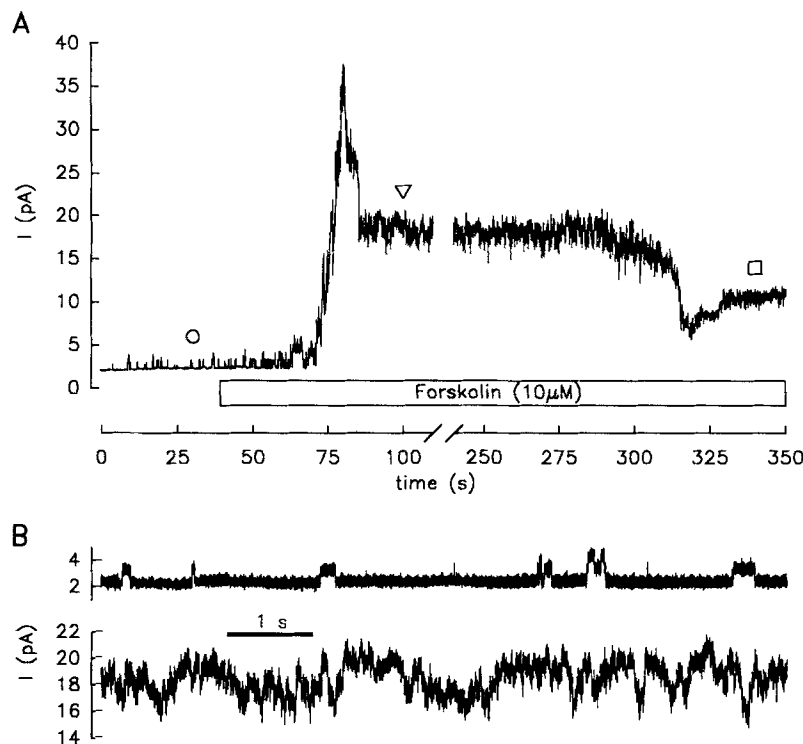


FIGURE 10. Stimulation of a cell-attached multichannel patch induces the high P_o gating mode. (A) Overview current trace sampled at 50 Hz; $V = 100$ mV; break in X-axis is 130 s with unchanged conditions. Note the very long opening of two channels shortly before the large increase of I . (B) 8-s sections from 8A replotted (sampled at 2 kHz, filtered at 500 Hz). Upper trace (taken from 8A at time = 41 s) shows unstimulated activity with long closed times ($\sigma^2 = 0.19$ pA²). Lower trace (taken from 8A at time = 276 s) shows current noise under stimulated conditions ($\sigma^2 = 1.32$ pA², $i = 0.85$ pA, $I = 16$ pA).

the temporary high P_o mode at the beginning of the overview trace. Stimulation increased both the total current and also the current variance immensely (Fig. 12 B, *bottom* trace), indicating a significant increase of gating activity. Therefore, the majority of channels were likely in the low P_o mode.

The quantification of the current noise of this recording is shown in Fig. 13. Spectra recorded under control (*circles*) and low dose forskolin-stimulated conditions (*triangles*) are shown in Fig. 13 A. The Lorentzian amplitudes increased greatly due

to the increased current noise. Fig. 13 *B* shows the change of σ^2 -data during stimulation. Note that the σ^2 -values were larger by one order of magnitude compared to Fig. 11 *A*. σ^2 showed a behavior typical for independent channels regulating their P_o after current stimulation, and thus followed a parabola of the form (Sigworth, 1980)

$$\sigma^2 = I \cdot i - I^2/N. \quad (6)$$

Fig. 13, *C* and *D*, show the changes of P_o and N with stimulation as calculated from the σ^2 -data. Stimulation of current was mainly due to an increase in P_o with a maximum in this record of $P_o \sim 0.6$, while N remained, once the channels were

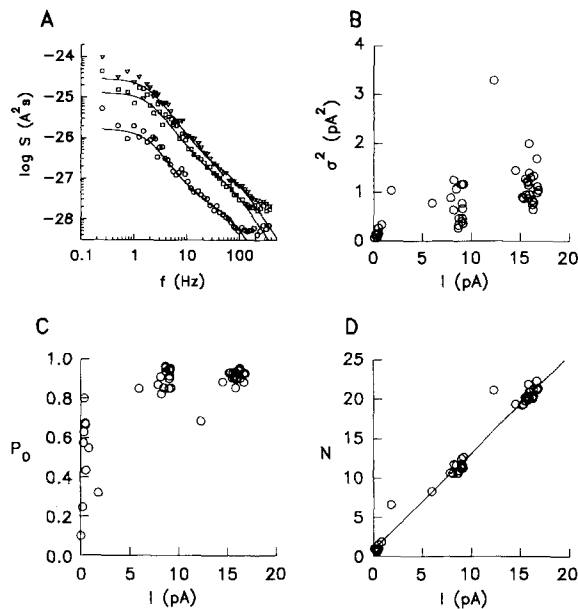


FIGURE 11. Noise analysis of the multichannel recording in Fig. 8. (*A*) Current noise spectra were recorded at the times indicated by the symbols in 8*A* and correspond to the same three symbols of spectra. All spectra were fitted with a double Lorentzian. Increased noise at high frequencies (> 150 Hz) was omitted for fits. Fitted values are ($f_c, f_{ch}, S_{ol}, S_{oh}$): (circle) 1.75 Hz, 46.1 Hz, $16.8E-27$ A²s, $0.234E-27$ A²s; (triangles) 1.81 Hz, 43.6 Hz, $299E-27$ A²s, $2.68E-27$ A²s; (squares) 1.98 Hz, 48.9 Hz, $131E-27$ A²s, $1.35E-27$ A²s. Lorentzian variances were 0.063 pA², 1.03 pA², and 0.511 pA², respectively. (*B*) Variance

(σ^2) and current (I) were calculated from 10-s intervals from the current trace filtered at 200 Hz. (*C*) P_o as calculated from σ^2 -data with Eq. 3. Note that the P_o reports an average value from channels in both gating modes. (*D*) N as calculated from σ^2 -data with eq. 4. N correlates closely with I ($r = 0.990$, $n = 48$, $p < 0.001$) and is the major regulator of current after stimulation.

activated, relatively constant. These observations indicate that the channels in this recordings were largely in the low P_o mode, where P_o was the major regulator of current. These results are in marked contrast to the recording shown in Fig. 10 where, once CFTR had switched to the high P_o mode, current was regulated largely through changes in N (Fig. 11 *D*).

Modal Switching

Having shown that the CFTR exists in two distinct gating modes and that during stimulation channels switch from the low P_o mode to the high P_o mode, it appeared likely that modal switching represented an effective means to regulate Cl^- current.

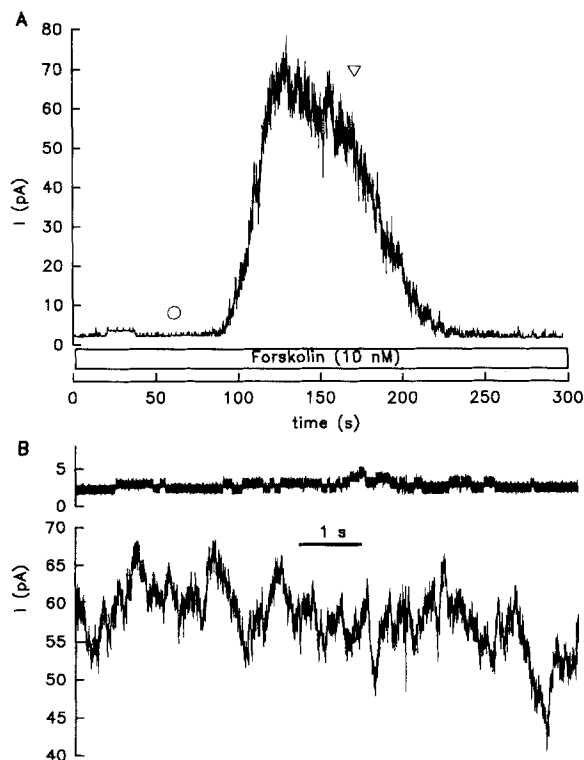
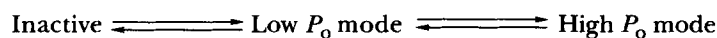


FIGURE 12. During low dose forskolin stimulation of a cell-attached patch, most of the activated channels remain in the low P_o mode. (A) Overview current trace, sampled at 50 Hz, $V = +80$ mV, $i = 0.64$ pA. Note the high P_o mode at the beginning of the trace. The two symbols denote the times where corresponding spectra in Fig. 13 A were recorded (B) Details of A taken at 8 s (top trace, $\sigma^2 = 0.26$ pA²) and 147 s (bottom trace, $\sigma^2 = 17.7$ pA²), filtered at 500 Hz.

The high P_o mode was observed more frequently in cells that had been stimulated maximally with high forskolin concentrations. 11 out of 15 recordings (73%) which expressed the high P_o mode continuously or temporarily were stimulated with 10 μ M forskolin (examples are Figs. 8, A and B, and 10). Of 11 recordings which showed exclusively channels in the low P_o mode, only one (9.1%) was stimulated with a high (10 μ M) forskolin-dose and all others with lower (<1 μ M) concentrations. The high P_o mode exhibited no apparent voltage dependence because it was observed in recordings at both positive ($n = 10$) and negative ($n = 5$) potentials.

The two gating modes were not mutually exclusive, as shown in Figs. 8 A, 10, and 12. Channels appeared often to switch modes, and, as displayed in Fig. 8 B, the high P_o mode was frequently observed during the initial stimulation of the cell. Due to the forskolin-dependence of these results, modal switching may be controlled by the phosphorylation/dephosphorylation state of the CFTR. In addition, we observed the high P_o mode only in multichannel patches, indicating a need for cross-talk, probably between channel pairs, for modal switching.

Transitions among the different gating modes of CFTR can tentatively be described by the following model



MODEL II

where transitions to a higher P_o mode (to the right) probably involve phosphorylation, and to a lower P_o mode, dephosphorylation. Approximate P_o values are $P_o \sim 0$ for the inactive state, $P_o \sim 0.5$ for the low P_o mode, and $P_o \sim 1.0$ for the high P_o mode.

DISCUSSION

Experimental Conditions and Methodology

The purpose of this study was to determine the characteristics of the CFTR during stimulation. We chose the experimental conditions to closely resemble physiological

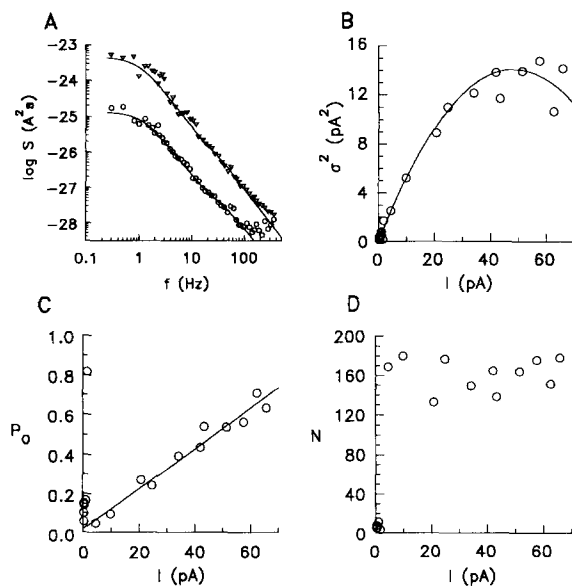


FIGURE 13. Noise analysis of multichannel recording in Fig. 12. (A) Stimulation increased the Lorentzian amplitudes but did not significantly affect corner frequencies. Fitted Lorentzian parameters are (f_{cl} , f_{ch} , S_{0l} , S_{0h}): control (circles) 1.21 Hz, 41.6 Hz, $0.13E-24$ A²s, $0.32E-27$ A²s, $\sigma^2 = 0.268$ pA², and stimulated (triangles) 1.0 Hz, 28.9 Hz, $4.69E-24$ A²s, $5.76E-27$ A²s, $\sigma^2 = 7.63$ pA². Increased noise at high frequencies (> 150 Hz) was omitted for fits. (B) With stimulation of I , the σ^2 followed Eq. 6 (continuous line) indicative for independent gating in this recording. σ^2 and I was calculated

from 10-s intervals filtered at 200 Hz. (C) After stimulation P_o (as calculated from Eq. 3) correlated closely with I and was the major regulator of Cl^- current ($r = 0.981$, $n = 11$, $p < 0.001$). (D) N (as calculated from Eq. 4) remained essentially unchanged after the initial stimulation.

conditions, i.e., constant bath perfusion, constant temperature of 37°C, stimulation with a single agonist, and, most of all, the cell-attached patch clamp mode, which allowed us to reliably stimulate the CFTR with forskolin. We have noticed that CFTR's gating is significantly changed after patch excision. Specifically, after excision of forskolin-stimulated patches into ATP-containing solution, the fast Lorentzian was greatly diminished as well as its voltage dependence. Addition of the catalytic subunit of protein kinase A did not appear to circumvent this loss of fast gating after excision (Fischer and Machen, unpublished results). Qualitatively similar observations have also been reported by others (Cliff, Schoumacher, and Frizzell, 1992; Haws et al., 1992; Haws, Finkbeiner, Widdicombe, and Wine, 1994). Therefore, we hypothesize that unknown cellular factors are associated with the CFTR in vivo, which get

disturbed by excision. Evidence for CFTR-associated factors has been presented previously (Becq, Fanjul, Merten, Figarella, Hollande, and Gola, 1993).

Because the CFTR is a small (5–10 pS) Cl⁻ channel, it must be present in high abundance to accomplish normal rates of Cl⁻ secretion in epithelial cells. This has made it difficult to study channel gating and regulation by classical single-channel event analysis. This problem significantly reduced the number of recordings we could use for event analysis, and also limited the bandwidth for data analysis in order not to introduce nonspecific noise. The major use of single-channel analysis, therefore, was for assessing the slow events. We applied stationary noise analysis and variance analysis to multi-channel recordings to overcome these limitations of single-channel analysis. This allowed us to better quantify the fast gating of the CFTR, and to calculate P_o and N of recordings. Exploiting the advantages of single-channel analysis in the low-frequency range and of noise analysis in the high-frequency range allowed us to cover a wide spectrum of channel gating and deal with the large numbers of channels in a recording, which, as we showed in this report, was advantageous for characterizing CFTR's regulation.

Note that Larsen et al. (1992, 1993) reported an additional Lorentzian of ~ 0.5 Hz in CFTR-transfected SF9-cells. This very slow Lorentzian may relate to the long closings we have found in single-channel recordings. This Lorentzian was too slow to be resolved in our bandwidth of noise analysis. Variances calculated from longer, 10-s intervals show higher values than the Lorentzian variances (compare Fig. 13, *A* and *B*), suggesting additional low frequency noise. Visual inspection of current traces in Figs. 3 *A*, 10 *B*, and 12 *B* similarly suggest frequencies lower than 1 Hz.

Due to CFTR's complicated kinetics (especially the long closed times and the two gating modes), the estimation of P_o from single-channel analysis is difficult, and channels which open for very long times (see Fig. 6 *B*) may easily be missed. To avoid this problem, we stimulated silent, cell-attached patches. This approach allowed us to verify the current baseline. Haws et al. (1992) tackled this difficulty by excising cell-attached, multichannel patches, which lead to an inactivation of channels. Using this approach, the zero-current level was determined, and channels expressing high P_o -values were similarly reported (Haws et al., 1992).

Voltage Dependence of the CFTR

Voltage dependence of the CFTR was somewhat controversial because in whole-cell recordings, currents varied reasonably linear with voltage and the single-channel conductance in excised patches is linear with symmetrical Cl⁻ concentrations (Gray, Harris, Coleman, Greenwell, and Argent, 1989; Cliff and Frizzell, 1990; Dalemans et al., 1991). Therefore, $N \cdot P_o$ of CFTR was expected to be independent of voltage. Single-channel gating kinetics, however, were found to be voltage dependent in cell-attached patches, i.e., fast gating dominated at negative potentials (Cliff et al., 1992; Haws et al., 1992).

Quantification of CFTR's gating kinetics have been hampered by problems associated with classical single-channel analysis. We quantified the voltage-dependent gating in noise-analytical terms. We found that the fast Lorentzian increased its corner frequency from 44 Hz at +100 mV to 92 Hz at -100 mV and at the same time increased its variance fourfold (Fig. 3, *C* and *D*). Although we have also detected the

voltage dependence in single-channels records, the voltage-dependent time constants ($\tau_{\text{om}} = 62.7 \pm 3.3$, $\tau_{\text{cs}} = 4.9 \pm 0.15$) significantly underestimated the observed corner frequencies ($f_{\text{ch}} = 91.8 \pm 6.8$ Hz) in the noise spectra. We suspect that the apparent discrepancy is due to the fact that the short closed time constant from our single-channel analysis might be overestimated, because it lays at the edge of our time resolution for single-channel event analysis. To yield the given fast Lorentzian, with $2\pi f_c = 1/\tau_o + 1/\tau_c$, a $\tau_{\text{cs}} = 1.8$ ms can be predicted at -100 mV.

In addition we have found a significant voltage dependence of $N \cdot P_o$. Interestingly, we observed both changes in P_o (likely due to the changes in fast gating) and changes in N (channel recruited from an electrically silent pool). With this voltage dependence, currents carried by the CFTR should be expected to show outward rectification. Since neither current noise nor currents were reported as voltage dependent, the quite different recording conditions between cell-attached and whole-cell mode might have obscured this relation.

Once the channel is activated the fast, voltage-dependent gating of CFTR in the low P_o mode is not regulated (i.e., affected by forskolin; Fig. 7), so, we conclude that these states are spontaneous conformational changes of the protein. One molecular candidate for voltage effects on channel gating is the R domain, the part of the CFTR expressing multiple phosphorylation consensus sites (Riordan et al., 1989). Given that the R domain is phosphorylated after stimulation (Cheng, Rich, Marshall, Gregory, Welsh, and Smith, 1991), it carries a high negative charge. In a simple mechanistic model, a negative potential (applied by the patch pipette or the negative cell potential) would force the negatively charged R domain into the membrane, which might obstruct the CFTR pore and induce gating events comparable to a fast blocker. At positive potentials, the R domain would be pulled away from the membrane, thereby reducing the fast gating. This hypothesis is consistent with the recent finding that the R domain appears to interact electrostatically with the pore after phosphorylation (Rich, Berger, Cheng, Travis, Saxena, Smith, and Welsh, 1993). Another possibility is that there are cellular factors that interact with the CFTR, and these factors are lost in excised or whole cell recording mode, leading to the loss of voltage-dependent gating.

*Regulation of the CFTR: Independent Low P_o and Cooperative
High P_o Gating Modes*

Forskolin stimulation caused two major modifications of CFTR's function: (a) Regulation of the long closed state in the low P_o mode, and (b) switching of the gating mode from the low P_o to the high P_o mode.

Most previous studies have described exclusively the low P_o mode of CFTR, which is characterized by independent gating and P_o values of ~ 0.5 . For example, Venglarik et al. (1994) have reported independent gating of excised CFTRs with a stimulated P_o of 0.45 in a noise analytical study of single channels expressed in mouse L-cells. Likewise, Haws et al. (1992) showed amplitude-histograms of cell-attached and excised-, multichannel records of CFTR which did not significantly deviate from a binomial distribution, indicating independent channels. Early on,

Gray et al. (1989) reported that P_o of CFTR increased from 0.08 to 0.28 after secretin-stimulation of pancreatic duct cells, and Dalemans et al. (1991) found a P_o of 0.35 in CFTR-expressing Vero cells. These results are all consistent with CFTR operating solely in the low P_o mode described in our study.

In addition, we found evidence consistent with CFTR operating in a cooperative high P_o mode (i.e., P_o approaches 1.0). Based on the observation that pairs of channels simultaneously entered the high P_o mode, we propose direct channel-channel interaction which is initiated by stimulation. Interestingly, Ko, Thomas, Delannoy, and Pedersen (1993) found that peptides, corresponding to the two nucleotide binding folds of the CFTR, formed polymeric structures, and concluded that the CFTR might exist as a multimer. A fundamental change in CFTR's conformation after modal switching is also indicated by the strikingly different gating behavior of the two modes, i.e., the prominent gating in the low P_o mode versus little detectable gating in the high P_o mode suggests that the structure defining the "gate" of the channel changed its functional effects dramatically.

Data consistent with the cooperative high P_o mode of CFTR have also recently been accumulating from other electrophysiological studies. For example, we presented evidence consistent with the possibility that the CFTR expresses an extremely high P_o in HT-29 epithelia (Fischer et al., 1992): From noise analysis of forskolin-stimulated transepithelial Cl^- secretion, we found that a slowly gating channel ($f_c = 1.4 \pm 0.2$ Hz) was responsible for stimulated currents, and the data were only consistent with CFTR's conductance (~ 9 pS) if its P_o was $\sim 0.95^1$. These transepithelial data (Fischer et al., 1992) compare very well to the single-channel data presented here and lead us to conclude that the high P_o mode of CFTR also occurs physiologically during transepithelial Cl^- secretion.

Cooperative openings of many CFTRs (Haws et al., 1992) and slow, wavelike, loosely coordinated currents of multiple channels (Kartner et al., 1991) have previously been observed. Larsen and co-workers (1992, 1993) have reported multiple conductance steps in single-channel recordings of CFTR which are consistent with openings in pairs, as we propose here.

CFTR's Structure-Function Relationship

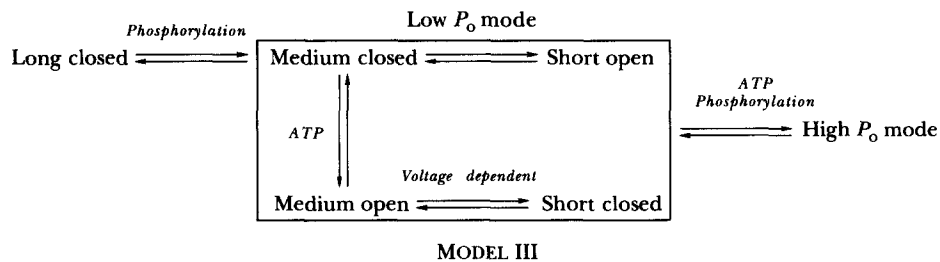
The primary structure of the CFTR predicts multiple phosphorylation sites and two nucleotide binding sites, allowing functional schemes which involve regulation by both phosphorylation and ATP binding. Given that forskolin-addition activates protein kinase A which, in turn, likely phosphorylates the channel, our data predict at least two functionally distinct phosphorylation events, the regulation of the long closed state and the switching to the high P_o mode. Similarly, Hwang, Horie, and Gadsby (1993) have attributed the stimulation of cAMP-regulated Cl^- currents in myocytes to sequential phosphorylation events. Employing the phosphatase inhibitor

¹ In a previous report (Fischer et al., 1992) we concluded from transepithelial Lorentzian noise that sub-picosiemens channels were responsible for this gating component. i was calculated with $i = (\pi f_c S_o) / (2 I [1 - P_o])$ which made it necessary to estimate P_o . The P_o of CFTR was then widely reported as ~ 0.5 leading us to conclude that i was very small. In the light of this present report, which shows the same slow Lorentzian and at the same time reports CFTR's conductance and P_o , we conclude in retrospect that P_o of CFTR is also very high in intact epithelia.

okadaic acid they dissected the forskolin stimulation of whole-cell currents into two distinct and sequential phosphorylation events which might reflect different P_o 's of the CFTR.

ATP also modulates CFTR activity. Venglarik et al. (1994) have shown in a recent noise analytical study of CFTR excised from transfected fibroblasts that the low frequency Lorentzian was dependent on the ATP concentration. These results indicate that ATP modulates the medium open-medium closed-transition in our gating model (Model I). It has also been shown that ATP binding to the two nucleotide binding folds had distinct functional effects on CFTR activation kinetics expressed in frog oocytes (Smit, Wilkinson, Mansoura, Collins, and Dawson, 1993). Hwang, Nagel, Nairn, and Gadsby (1994) exploited the different affinities of the two ATP-binding sites to the ATP-analog AMP-PNP to demonstrate the serial nature of ATP binding during regulation which appeared to be dependent on the level of phosphorylation. They concluded that incremental phosphorylation differentially regulates the availability of the ATP-binding sites, and that full phosphorylation and binding of ATP at both binding sites is required for optimal channel activity.

Adding the molecular information to the Models I and II results in the following scheme for the effectors of CFTR's gating:



The high P_o state was not connected to a specific state in this scheme because it was not obvious from our data. It is likely that phosphorylations elicit the transitions from the long closed to the medium closed state and from the low P_o to the high P_o mode because those transitions were dependent on forskolin stimulation. The reasoning for the two ATP-dependent transitions was pointed out above.

In conclusion, this report has shown that the CFTR exists in distinct states after stimulation: a low P_o mode with $P_o \sim 0.5$, and a high P_o mode in which CFTR pairs remain open for extended periods, with P_o approaching 1.0. Because forskolin stimulation regulated a modal transitions (low P_o to high P_o) and the longest closed state within the low P_o mode, it appears likely that these effects were elicited through different levels of phosphorylation. The high P_o mode of CFTR provides the state of maximal activation of Cl^- secretion.

We are grateful to Harold Lecar and Peter Larsson for helpful discussions during the course of the study and for thoroughly reading and commenting on the manuscript.

Horst Fischer is a Postdoctoral Fellow of the Cystic Fibrosis Foundation. This study was supported in part by the Cystic Fibrosis Foundation and Cystic Fibrosis Research, Inc.

Original version received 23 December 1993 and accepted version received 18 April 1994.

REFERENCES

- Anderson, M. P., D. P. Rich, R. J. Gregory, A. E. Smith, and M. J. Welsh. 1991. Generation of cAMP-activated chloride currents by expression of CFTR. *Science*. 251:679–682.
- Bear, C. E., F. Duguay, A. L. Naismith, N. Kartner, J. W. Hanrahan, and J. R. Riordan. 1991. Cl⁻ channel activity in *Xenopus* oocytes expressing the cystic fibrosis gene. *Journal of Biological Chemistry*. 266:19142–19145.
- Becq, F., M. Fanjul, M. Merten, C. Figarella, E. Hollande, and M. Gola. 1993. Possible regulation of CFTR-chloride channels by membrane-bound phosphatases in pancreatic duct cells. *Federation of European Biochemical Societies Letters*. 327:337–342.
- Cheng, S. H., D. P. Rich, J. Marshall, R. J. Gregory, M. J. Welsh, and A. E. Smith. 1991. Phosphorylation of the R domain by cAMP-dependent protein kinase regulates the CFTR chloride channel. *Cell*. 66:1027–1036.
- Cliff, W. H., and R. A. Frizzell. 1990. Separate Cl⁻ conductances activated by cAMP and Ca²⁺ in Cl⁻-secreting epithelia. *Proceedings of the National Academy of Sciences, USA*. 87:4956–4960.
- Cliff, W. H., R. A. Schoumacher, and R. A. Frizzell. 1992. cAMP-activated Cl channels in CFTR-transfected cystic fibrosis pancreatic epithelial cells. *American Journal of Physiology*. 262: C1154–C1160.
- Colquhoun, D., and F. J. Sigworth. 1983. Fitting and statistical analysis of single channel records. In *Single Channel Recording*. B. Sakmann, and E. Neher, editors. Plenum Publishing Corp., NY. 191–263.
- Dalemans, W., P. Barbry, G. Champigny, S. Jallat, K. Dott, D. Dreyer, R. G. Crystal, A. Pavirani, J. P. Lecocq, and M. Lazdunski. 1991. Altered chloride ion channel kinetics associated with the $\Delta F508$ cystic fibrosis mutation. *Nature*. 354:526–528.
- Datnyer, N. B., G. A. Gintant, and I. S. Cohen. 1985. Versatile temperature controlled tissue bath for studies of isolated cells using an inverted microscope. *Pflügers Archiv*. 403:318–323.
- Ehrenstein, G., H. Lecar, and R. Nossal. 1970. The nature of the negative resistance in bimolecular lipid membranes containing excitability-inducing material. *Journal of General Physiology*. 55:119–133.
- Fischer, H., K. M. Kreusel, B. Illek, T. E. Machen, U. Hegel, and W. Clauss. 1992. The outwardly rectifying Cl⁻ channel is not involved in cAMP-mediated Cl⁻ secretion in HT-29 cells: evidence for a very-low-conductance Cl⁻ channel. *Pflügers Archiv*. 422:159–167.
- Fischer, H., and T. E. Machen. 1993. Single channel and noise analysis of forskolin-stimulated CFTR. *Pediatric Pulmonology*. (Suppl.)9:214.
- Gabriel, S. E., E. M. Price, R. C. Boucher, M. J. Stutts. 1992. Small linear chloride channels are endogenous to nonepithelial cells. *American Journal of Physiology*. 263:C708–C713.
- Gray, M. A., A. Harris, L. Coleman, J. R. Greenwell, and B. E. Argent. 1989. Two types of chloride channel on duct cells cultured from human fetal pancreas. *American Journal of Physiology*. 257:C240–C251.
- Haws, C., M. E. Krouse, Y. Xia, D. C. Gruenert, and J. J. Wine. 1992. CFTR channels in immortalized human airway cells. *American Journal of Physiology*. 263:L692–L707.
- Haws, C., W. E. Finkbeiner, J. H. Widdicombe, and J. J. Wine. 1994. CFTR in Calu-3 human airway cells: channel properties and role of cAMP-activated Cl⁻ conductance. *American Journal of Physiology*. In press.
- Hwang, T.-C., M. Horie, and D. C. Gadsby. 1993. Functionally distinct phospho-forms underlie incremental activation of protein kinase-regulated Cl⁻ conductance in mammalian heart. *Journal of General Physiology*. 101:629–650.

- Hwang, T.-C., G. Nagel, A. C. Nairn, and D. C. Gadsby. 1994. Differential regulation of nucleotide binding sites in CFTR PKA phosphorylation. *Biophysical Journal*. 66:A141. (Abstr.)
- Kartner, N., J. W. Hanrahan, T. J. Jensen, A. L. Naismith, S. Z. Sun, C. A. Ackerley, E. F. Reyes, L. C. Tsui, J. M. Rommens, and C. E. Bear. 1991. Expression of the cystic fibrosis gene in non-epithelial invertebrate cells produces a regulated anion conductance. *Cell*. 64:681–691.
- Kerem, B., J. M. Rommens, J. A. Buchanan, D. Markiewicz, T. K. Cox, A. Chakravarti, M. Buchwald, and L. C. Tsui. 1989. Identification of the cystic fibrosis gene: genetic analysis. *Science*. 245:1073–1080.
- Ko, Y. H., P. J. Thomas, M. R. Delannoy, and P. L. Pedersen. 1993. The cystic fibrosis transmembrane conductance regulator. Overexpression, purification, and characterization of wild type and $\Delta F508$ mutant forms of the first nucleotide binding fold in fusion with the maltose-binding protein. *Journal of Biological Chemistry*. 268:24330–24338.
- Larsen, E. H., S. E. Gabriel, J. Fullton, R. C. Boucher, E. Price, and M. J. Stutts. 1992. Power density spectrum and single channel activity associated with CFTR mediated Cl^- currents. *The Physiologist*. 35:A1 (Abstr.)
- Larsen, E. H., S. E. Gabriel, J. Fullton, R. C. Boucher, E. Price, and M. J. Stutts. 1993. Multiple single channel conductances and gating time constants of CFTR-mediated chloride currents. *FASEB Journal*. 7:A426 (Abstr.)
- Lindemann, B. 1980. The beginning of fluctuation analysis in epithelial ion transport. *Journal of Membrane Biology*. 54:1–11.
- Rich, D. P., H. A. Berger, S. H. Cheng, S. M. Travis, M. Saxena, A. E. Smith, and M. J. Welsh. 1993. Regulation of the CFTR Cl^- channel by negative charge in the R domain. *Journal of Biological Chemistry*. 268:20259–20267.
- Riordan, J. R., J. M. Rommens, B. Kerem, N. Alon, R. Rozmahel, Z. Grzelczak, J. Zielenski, S. Lok, N. Plavsic, and J. L. Chou. 1989. Identification of the cystic fibrosis gene: cloning and characterization of complementary DNA. *Science*. 245:1066–1073.
- Rommens, J. M., M. C. Iannuzzi, B. Kerem, M. L. Drumm, G. Melmer, M. Dean, R. Rozmahel, J. L. Cole, D. Kennedy, and N. Hidaka. 1989. Identification of the cystic fibrosis gene: chromosome walking and jumping. *Science*. 245:1059–1065.
- Sachs, F., J. Neil, and N. Barkakati. 1983. The automated analysis of data from single ionic channels. *Pflügers Archiv*. 395:331–340.
- Sigworth, F. J. 1980. The variance of sodium current fluctuations at the node of ranvier. *Journal of Physiology*. 307:97–129.
- Sigworth, F. J., and S. Sine. 1987. Data transformation for improved display and fitting of single channel dwell time histograms. *Biophysical Journal*. 52:1047–1054.
- Smit, L. S., D. J. Wilkinson, M. K. Mansoura, F. S. Collins, and D. C. Dawson. 1993. Functional roles of the nucleotide binding folds in the activation of the cystic fibrosis transmembrane conductance regulator. *Proceedings of the National Academy of Sciences, USA*. 90:9963–9967.
- Tilly, B. C., M. C. Winter, L. S. Ostedgaard, C. O'Riordan, A. E. Smith, and M. J. Welsh. 1992. Cyclic AMP-dependent protein kinase activation of cystic fibrosis transmembrane conductance regulator chloride channels in planar lipid bilayers. *Journal of Biological Chemistry*. 267:9470–9473.
- Van Driessche, W., and W. Zeiske. 1980. Ba^{2+} induced conductance fluctuations of spontaneously fluctuating K^+ channels in the apical membrane of frog skin. *Journal of Membrane Biology*. 56:32–42.
- Venglarik, C. J., B. D. Schultz, R. A. Frizzell, and R. J. Bridges. 1994. ATP alters current fluctuations of cystic fibrosis transmembrane conductance regulator: evidence for a three state activation mechanism. *Journal of General Physiology*. In press.